PNNL-34948

Room Temperature Electrorefining of Rare Earth Metals from End-of-use Nd-Fe-B Magnets

September 2023

1 Hyung-Seok Lim
2 Chinmayee V Subban
3 Dan Thien Nguyen
4 Tasya S Nasoetion
5 Tingkun Liu
6 Kee Sung Han
7 Bhuvaneswari M Sivakumar
8 Teresa Lemmon
9 Soowhan Kim
10 Zhaoxin Yu
11 Arun Devaraj
12 Mark J Willey
13 Wei Wang
14 Vijayakumar Murugesan

Prepared for the U.S. Department of Energy
under Contract DE-AC05-76RL01830

PACIFIC NORTHWEST NATIONAL LABORATORY
operated by
BATTELLE
for the
UNITED STATES DEPARTMENT OF ENERGY
under Contract DE-AC05-76RL01830

Printed in the United States of America

Available to DOE and DOE contractors from
the Office of Scientific and Technical
Information,
P.O. Box 62, Oak Ridge, TN 37831-0062
www.osti.gov
ph: (865) 576-8401
fox: (865) 576-5728
email: reports@osti.gov

Available to the public from the National Technical Information Service
5301 Shawnee Rd., Alexandria, VA 22312
ph: (800) 553-NTIS (6847)
or (703) 605-6000
email: info@ntis.gov
Online ordering: http://www.ntis.gov

PNNL-34948

Room Temperature Electrorefining of Rare Earth Metals from End-of-use Nd-Fe-B Magnets

September 2023

1 Hyung-Seok Lim
2 Chinmayee V Subban
3 Dan Thien Nguyen
4 Tasya S Nasoetion
5 Tingkun Liu
6 Kee Sung Han
7 Bhuvaneswari M Sivakumar
8 Teresa Lemmon
9 Soowhan Kim
10 Zhaoxin Yu
11 Arun Devaraj
12 Mark J Willey
13 Wei Wang
14 Vijayakumar Murugesan

Prepared for
the U.S. Department of Energy
under Contract DE-AC05-76RL01830

Pacific Northwest National Laboratory
Richland, Washington 99354

Abstract

Recovering rare earth elements (REE) from used permanent magnets, which contains about 30 wt.% of rare earth elements, has been persistent technological challenge. Current recycling methods relies on pyrometallurgical or hydrometallurgical processes which are energy- and chemical- intensive and not economically and environmentally viable for rare earth containing magnets. Enabling efficient and simplistic recovery and refining of REEs contained in End-of-Use (EoU) products, such as Neodymium-Iron-Boron (Nd-Fe-B) based magnets will play an important and complementary role in the total supply of REEs in the future. We designed a new electrochemical method and demonstrated a room temperature one-pot process that concurrently separates and electroplates REE from commercial Nd-Fe-B magnets. By establishing selective oxidation and reductive potential as electrochemical control parameter along with electrochemically compatible non-aqueous electrolyte system, we demonstrated selective electroleaching of lanthanides (Nd and Preseodymium (Pr)) from anode and concurrent plating as alloy at Pt cathode. The morphological and chemical evolution of the Nd-Fe-B magnets during electroleaching reveals the electrochemical stimuli and rate of dissolution depends on microstructural complexities of the Nd-Fe-B magnet. The concomitant electroplating process leads to Nd-Pr based alloy which can be used as raw metallic alloy for manufacturing new permanent magnet and other devices. Our study demonstrates a scalable separation and refining methodology, based on widely available organic electrolyte system and without any consumptive chemical use, for selective lanthanide recovery from waste magnets.

Summary

Herein, we demonstrated a room-temperature one-pot electrochemical process that can selectively separate and concurrently deposit lanthanide elements as metallic alloy from commercial Nd-Fe-B magnets. Selective electrochemical leaching of lanthanides from Nd-Fe-B was achieved in aprotic organic solvent system which enabled concurrent electrodeposition of Ln-elements as metallic alloy system. We evaluated the electrochemical potential as control parameter to establish continuous leaching and deposition process under LiCl/DMF based electrolyte conditions. The spectroscopy and microscopy analysis of the deposition reveals Nd-Pr based didymium alloy which can be easily used as feedstock in production of new magnets and other REM based products. Our studies also suggest further electrochemical parameter and electrolyte material optimization can lead to better control over the Ln-element leaching from variant microstructural regions and metal nucleation processes. In particular, we envision the following advances can accelerate this technology transferred to industry, 1) an electrolyte design methodology to tune the redox potentials and kinetics and thereby control rate of REE dissolution and deposition, and 2) correlation of electrochemical stimuli (potential, pulse amplitude, and duration) to dissolution and deposition processes of REEs and thereby control selectivity. Overall, we demonstrated an electrochemical methodology, which can be rapidly and sustainably scaled-up within existing industrial infrastructure and offers a viable waste-free and circular manufacturing of critical metals from electronic and industrial wastes.

Acknowledgments

This research was supported by the Energy Storage Materials Initiative (ESMI), under the Laboratory Directed Research and Development (LDRD) Program at Pacific Northwest National Laboratory (PNNL). PNNL is a multi-program national laboratory operated for the U.S. Department of Energy (DOE) by Battelle Memorial Institute under Contract No. DE-AC05-76RL01830.

Contents

Figures

Tables

1.0 Introduction

The Neodymium-Iron-Boron (Nd-Fe-B) alloy based permanent magnet is ubiquitous component of modern energy technologies, ranging from industrial motors and automation, consumer electronics and wind turbines. The size of these magnets ranges from less than 1 g in portable electronics to well over 1000 kg in the generators of wind turbines, with each magnet containing about 32 wt.% of rare earth metals (REMs) such as neodymium (Nd), dysprosium (Dy) and praseodymium (Pr). Despite being readily available feedstock, that could help establish domestic circular supply chain for rare earth elements (REEs), no large-scale recovery processes are currently established for recycling End-of-Use (EoU) magnets. [1] A foremost reason for the absence of any major efforts for recycling of these magnets is technological challenges associated with separation and refining of REMs. The current methodologies to recover REEs are based on traditional hydro- and pyro- metallurgy which are energy and chemical intensive, comes with high environmental and economic cost. Even then, the recovered rare earth elements are often in oxidized form (Ln^{3+}) necessitating re-metallization[2] process through high temperature (≥500°C) electrowinning or metallothermic reduction, adding further environmental and economic cost of recycling process. Developing a single step ambient temperature electrochemical recovery process, that encompasses both separation and refining of REEs in metallic form, with atom and energy efficiency, can reduce industrial energy consumption and CO_2 emission, as well as provide pathway for domestic circular supply chain. Electrochemical methods for recovery of REEs from EoU magnets have been explored as shown in the technical flow chart (Figure 1), but primarily focused on electrolytic dissolution in aqueous acidic electrolyte systems. For example, EoU Nd-Fe-B based magnets are subjected to electrolytic dissolution in strong mineral acid (HCl, HF or H_2SO_4)[2-4] or organic acid (acetic or citric acid) [5, 6] based electrolytes to separate the Nd ions. The dissolved aqua-Nd ions are then selectively separated from other constituents either by solvent extraction,[5, 7, 8] membrane-assisted solvent extraction, [8, 9] or membrane electrolysis. [4] The dissolved Nd ions were subsequently precipitated using oxalic acid followed by calcination at 800°C to obtain Nd_2O_3. [4, 5, 10]To convert the oxides back to metallic form, a necessary feedstock for magnetic alloys manufacturing, further electrochemical approaches such as high temperature molten-salt electrolysis,[11] and an iron electrodeposition in HF were used.[12] While these electrolytic separation or molten salt based REM deposition highlight the promise of electrochemical methods, these multi-step processes involves untenable chemical and energy waste leading to higher capital and operational cost for EoU magnet recycling.[10] The scientific challenges in achieving a combined electrochemical separation and refining of REMs are (1) very high negative redox potential of REEs, which leads to intense parasitic reactivity with electrolyte, and (2) high activation barriers for diffusion, hampering transport and transfer of trivalent ions (Ln^{3+}) across interfaces. Recent efforts are focused on exploring ionic liquids-based electrolytes which addresses high negative redox potential but suffers poor transport kinetics even with exogenous thermal energy (70–150 °C). Recently, inspired by multivalent battery research, an organic electrolyte with ether based solvent has been reported for room temperature electrodeposition of Nd using borohydride based precursor salt.[13] Although this study, based on well-defined Nd precursor salts, suggests the possibility of addressing reactivity and transport limitations of REM electrodeposition, the electrolytic dissolution of EoU magnet with real-world complexities would require greater control over selective dealloying process and subsequent deposition of complex REE precursors. Identifying optimal electrolyte system and electrochemical conditions that can handle real-world EoU magnets as precursors and effectively combine separation and refining into single process could be transformative technology for REEs circular supply chain. Herein, we demonstrate an efficient one-pot electrochemical process using common organic electrolytes to selectively dissolve REEs from commercial Nd-Fe-B magnets and concurrently deposit as REMs at room temperature (Figure 1). Our one-pot electrochemical cell setup recovers lanthanide (Ln) elements Nd and Pr through selective oxidation and reduction steps at anode and cathode respectively, as shown in Eq.1 & 2. We used demagnetized Nd-Fe-B magnets as REE source at anode and selectively electroplated Nd and Pr metals on platinum cathode with dimethylformamide (DMF) based electrolyte by carefully controlling the applied potentials.

$$[Ln - Fe - B]_s^0 \rightarrow [Ln]_l^{3+} + [Fe - B]_s + 3e \text{ - \textit{Anode (1)}} \qquad (1)$$

$$[Ln]_l^{3+} + 3e^- \rightarrow [Ln]_s^0 \text{ - \textit{cathode (2)}} \qquad (2)$$

The oxidation potential of lanthanides is about -2.3V (vs Ag/AgCl), which is significantly lower than the iron and boron, and thereby enables excellent selectivity in electrolytic dissolution through applied potential. The dissolved lanthanide ions i.e., $[Ln]_l^{3+}$ solvated by organic solvents exhibit higher transport properties and enables concurrent reduction at cathode resulting in deposition of didymium alloy (Nd and Pr based alloy widely used in magnets and glass filters manufacturing) under the one-pot condition with same oxidative dissolution potential. This electrochemical process represents a simplistic and room temperature electrorefining process for REMs with excellent atom and electron efficiency. Our approach eliminates need for chemical and thermal pretreatment of magnets and also yields as high-quality REM alloys (such as didymium alloy) which can be directly used as feedstock in production of commercial magnets and thereby enables a domestic circular supply chain economy for REEs.[14]

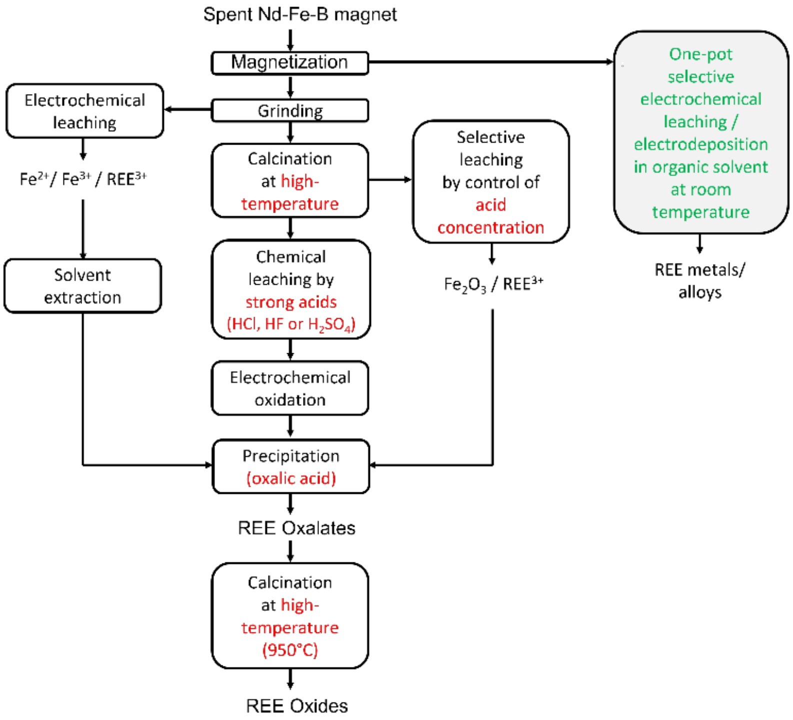

Figure 1. Flow chart of the typical electrochemical techniques and one-pot selective electrochemical leaching/deposition at room temperature for recycling REEs from spent Nd-Fe-B magnets.

2.0 Materials and methods

Materials

Lithium chloride (LiCl, 99.99%, battery grade) and N,N-Dimethylformamide (DMF, 99.8%, anhydrous) were purchased from Sigma-Aldrich. Platinum plate electrodes (Purity 99.99%), silver (99.99%) and platinum wires (99.99%) were used as electrodes after surface polishing. The Uncoated neodymium-iron-boron (Nd-Fe-B) permanent magnet rods (35NERR16-2, grade-35, diameter: 0.25 in, length: 2 in) were purchased from MagnetShop.com. The Nd-Fe-B discs were cut from the magnet rod using a diamond cutter and demagnetized by annealing at 400 °C for 30min in vacuum to avoid oxidation. The demagnetized samples were grinded using sandpapers up to 1200 grids to remove surface coatings. The finial polishing was done using a vibratory polisher in a 0.06μm amorphous colloidal silica suspension for 2-3 hours.

Electrochemical measurements

All electrochemical measurements were performed at ambient temperature conditions in the argon filled glovebox. The 3-electrode glass electrochemical cell (shown in Figure S1) used in the study contains polished Nd-Fe-B permanent magnetic rod as counter electrode, platinum (Pt) plate as working electrode, and a silver wire as pseudo reference electrode. The cell was filled with approximately 15 mL of 0.1 M LiCl/DMF electrolyte prior to voltage cycling in the different voltage ranges vs. Ag/Ag_2O. The surface of silver wire was polished and dried before use. Cyclic voltammetry (CV) measurements were performed using a potentiostat (GAMRY, Interface 1000). Polarization curves were recorded at a potential sweep rate of 20 mV/s and 5mV/s between -2.8 V to 1V vs. Ag/Ag_2O. Observed reduction and oxidation peaks were converted to standard reduction potential values (E°) using a modified Nernst equation ($E^\circ = E_{Ag/Ag_2O} + E^\circ_{Ag/Ag_2O}$), with $E^\circ_{Ag/Ag_2O} = 0.342$ V, and the assumption that there is not significant difference in pH between the experimental and standard reduction potential values. The chronoamperometry technique with constant potentials and over extended times were performed to investigate the effect of electrodeposition parameters on the selectivity and growth of the REMs on the platinum working electrode. The polished magnet discs (diameter: 0.2 in, thickness: 2 mm) connected with a Pt wire were used as a counter electrode. After the potentiostatic measurement, the electrodes were rinsed with fresh DMF and dried in a vacuum for the characterizations.

Characterization

The Scanning electron microscopy (SEM) coupled with Energy dispersive x-ray analysis (EDX), and X-ray photoelectron spectroscopy (XPS) were performed to analyze the morphology and composition of electro-dissolution and deposition products. The microstructure and associated elemental composition analysis was performed using FEI Quanta 3D FIB scanning electron microscopy (SEM) coupled with Energy dispersive x-ray analysis (EDX). The EDX elemental composition was characterized by the energy-dispersive X-ray spectroscopy at an accelerating voltage of 10KV. After electrochemical deposition, the Pt electrode was washed with a fresh DMF for 30 seconds and dried in Ar-fill glovebox with moisture and oxygen concentration below 5 ppm. The samples were then transferred to X-ray photoelectron spectroscopy (XPS) analysis chamber through in-built load-lock within glove box. The XPS data were collected using a Kratos Axis Ultra DLD spectrometer, which equipped with an Al Kα monochromatic X-ray source (1486.6 328 eV) and a high-resolution spherical mirror analyzer. X-ray source was operated at 150 W power and the emitted photoelectrons were collected at the analyzer entrance slit normal to the sample surface. The 2D XPS imaging data acquisition was carried out in a hybrid mode with analysis area of 800 × 800 μm^2. High energy resolution photoelectron spectra were collected using a pass energy of 40 eV with a step size of 0.1 332 eV. To remove the surface layer and study sub-surface chemical composition, the deposited sample was cleaned using 2 KeV Ar ion sputtering for 30min. The XPS spectra were analyzed using the CasaXPS software with mixed Gaussian/Lorentzian [GL (30)] line shape and Shirley background correction. The spectra were calibrated using Ag 3d signal at 368.2 eV. The main paragraph text follows directly on here.

3.0 Results and discussion

The first control parameter in recovering REEs from EoU magnet is to identify critical potential that can establish selective and steady state oxidative dissolution from intermetallic Nd-Fe-B alloy system.[15] It is known that the oxidative potentials of each alloy component strongly depend on the local composition and is always more positive than the corresponding potential of the individual metal. The magnet system is dominated by grains of $Nd_2Fe_{14}B$ intermetallic compound, where gadolinium (Gd), Pr and possibly other REEs along with other transition metals are substituted in the lattice of $Nd_2Fe_{14}B$ phase, leading to heterogeneous chemical distributions.[16] Beyond this compositional variances, Nd-rich phases with different crystal structures were also identified with Nd concentrations ranging from 70 to 90% rendering additional structural complexities.[17, 18] Finally, the EoU Nd-Fe-B magnets are known to have morphological diversity arising from grains, oxidized grain boundary regions and protective coatings encompassing multiple chemical and structural phases.[19] To unravel the structural and chemical complexity of commercial Nd-Fe-B product, we performed SEM based microscopic and compositional analysis on polished magnet as shown in Figure 2. The overall Ln composition is over 32 wt %, including ~20% of Nd, ~7.4% of Gd and ~4.6% of Pr, mostly concentrated as Ln-rich phases embedded across common iron rich $Nd_2Fe_{14}B$ phase separated by clear grain boundary, as shown in Figure 2b and c. Overall, the Nd-Fe-B magnet is embedded with structural and compositional heterogeneity ranging from atomistic to mesoscale making it challenging to establish oxidative potential through empirical formulations.

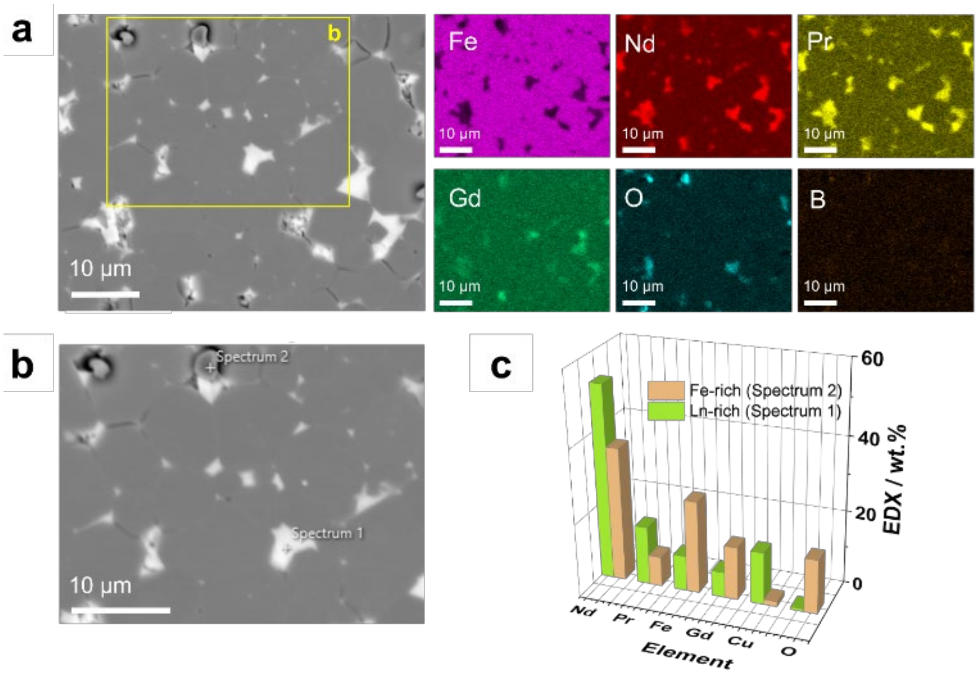

Figure 2. (a and b) SEM, elemental mapping and (c) EDX analysis of the polished Nd-Fe-B magnet sample. Region of the elemental mapping is marked in the yellow box of (a). Spots of Spectrum 1 and Spectrum 2 are highlighted in (b).

We performed cycling voltammetry (CV) over a wide potential range (-3.25V to 1.0V) for ten consecutive cycles at 20 mV/s scan rate using 0.1 M LiCl in DMF on a Pt electrode with Nd-Fe-B magnet as counter electrode and Ag/Ag_2O as reference electrode (Figure S2a). The first cycle CV representing the initial electroleaching process, shown in Figure 3c, clearly establishes the oxidative stripping reactions of Ln^{3+} such as Nd^{3+}, Gd^{3+} and Pr^{3+} around -2.25 V followed by with iron, a primary constituent of the magnet, around - 0.7 V. Although, the CV confirmed the applied potential as control parameter for selectively electroleaching of REEs from Nd-Fe-B magnet under the LiCl/DMF electrolyte condition, it is critical to establish continuous state electrodeposition at counter Pt electrode. The reductive platting potentials of REEs along with redox potentials of other chemical components of Nd-Fe-B magnet such as corrosion resistant layers and impurities at the Pt counter electrode are listed in supporting information (see Table S1). The CV measurement also revealed the reductive potential of Nd^{3+} and Nd^{2+} are around at -2.9 V and -2.58 V, respectively (Fig 2c) under DMF based electrolyte. The reduction reaction of borate and iron were observed at -1.11 V and at -0.72 V respectively. Relatively smaller reduction peaks representing aluminium and nickel were also observed at -1.66 V and -0.72 V respectively, indicating corrosion resistance layer in commercial magnets. This clear separation of reduction potentials among common constituents of commercial Nd-Fe-B based magnet further supports our hypothesis of establishing one-pot electrochemical separation and electrodeposition of Ln elements. The persistent challenge is to ensure the oxidative dissolution potential is optimal for selective and continuous Ln electrodeposition and within electrochemical stability of electrolyte system. Reductive potential scan shows multiple regions indicative of Nd^{3+} reduction to Nd^{2+} (region a) followed by Nd^{3+} and Nd^{2+} reduction to Nd^{2+} and Nd^0 respectively (region b). Oxidative potential scan shows Nd^0 and Nd^{2+} oxidations (region c) followed by and Nd^0 oxidation to Nd^{3+} and Nd^{2+} (region d). Other lanthanides, such as Pr and Gd will likely to overlap with these redox potentials and the detailed list of possible redox potentials of other elements from Nd-Fe-B magnet are given in supporting information (Table S1).

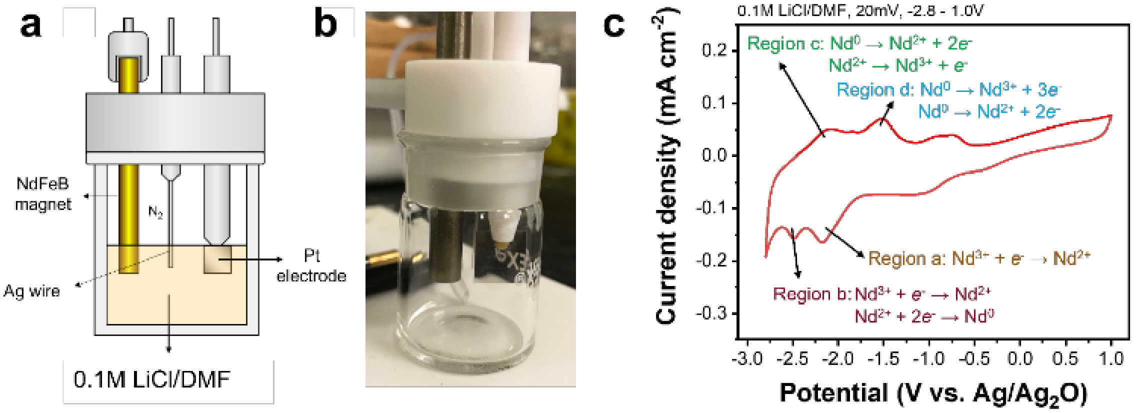

Figure 3. (a) Schematic illustration and (b) digital photograph of the one-pot electrochemical cell with commercial Nd-Fe-B magnet rod, platinum plate and silver wire in immersed in 0.1M LiCl/DMF based electrolyte for the cyclic voltammetry test and (c) cyclic voltammograms performed at a scan rate of 20mA s-1 in the potential range -2.8V – 1.0V vs. Ag/Ag_2O.

The CV measurement revealed the range of oxidative and reduction potentials for Ln-elements embedded within the chemical heterogeneity of Nd-Fe-B magnet but establishing a single oxidative dissolution potential with higher selectivity and columbic efficiency is critical first step for electrorefining. We have performed constant potential amperometry across various oxidative potential (from -0.3V to -3.3V) to establish higher columbic efficiency for selective Ln dissolution. The amperometry analysis, shown in Figure 4a, revealed that -3.3V potential registers higher current density implying continuous oxidative dissolution of Nd-Fe-B magnet. At -3.3V, the dissolution current reaches maximum of about 230μA after ~2hrs and then slowly reduces and establishing stable 85μA current after 14hr (see Figure 4a). This current evolution reveals that the rate of dissolution and deposition not only depends on the applied potential but could also depend on electrolyte stability and/or oxidative reaction front propagation mechanisms defined by multiphase grain boundary regimes of Nd-Fe-B system.[20] To evaluate the stability of LiCl/DMF electrolyte, we employed nuclear magnetic resonance spectroscopy (NMR) spectroscopy (Figure S3). The 1 H and 13 C NMR analysis of electrolyte after 24hr dissolution at -3.3V shows no detectable decomposition products indicating that the DMF based electrolytes are relatively stable for the constant potential amperometry conditions to concurrently dissolve and deposit the Ln ions. Previous corrosion and leaching studies under aqueous conditions noted similar phenomena, where the dealloying reaction front propagating through selective grain boundaries involving Nd-rich regions, while skipping some grains altogether.[10, 21, 22] Such selective dissolution pathways across grain boundary will be dictated by intra-grain solid-phase diffusion limitations, which is likely manifesting as gradual drop in dissolution current after 2hr (Figure 4a).

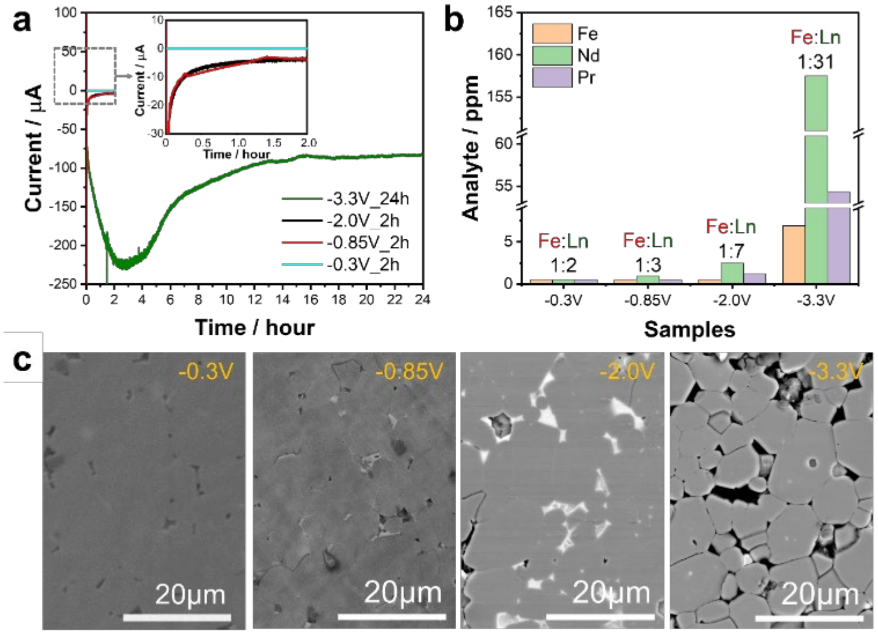

Figure 4. (a) Amperometric current responses of the working electrodes as a function of the applied potentials for 2 hours and (b) 24 hours at -3.3V. (c) ICP-OES analysis of REEs (Nd and Pr) and iron concentrations in the 0.1M LiCl/DMF electrolytes after the amperometry dissolution performed under different potentials for 2 hours and (c) corresponding SEM images of the magnet electrodes obtained after the same amperometry measurement.

To enable continuous dissolution process, it is essential to unravel the dissolving element, dissolution front and associated grain boundary regimes of Nd-Fe-B magnet. To identify the dissolving element, we performed ICP based compositional analysis of electrolytes after amperometry dissolution conditions shown in Figure 4b. It is clear that Ln elements (primarily Nd and Pr) are dominant solute with nearly 31:1 compositional ratio with Fe after 24hr of applied potential. The SEM images (Figure 4c) reveal Ln rich phases were mostly leached out at -3.3V while remain intact under higher potentials confirming selective oxidative leaching process. Although, this suggests highly selective dissolution of lanthanides it also raises the question about the origin of dissolving phase within Nd-Fe-B magnets. For example, the presence of iron in electrolyte suggests iron rich grains undergoing oxidative dissolution and/or becoming detached from Ln-rich grains due to dealloying of dominant alloy constituents. However, theoretically (vide infra) the oxidative potential of iron dissolution should be higher than 0.1V (i.e. $Fe(s) \rightarrow Fe^{2+} + 3^{e^-}$ vs Ag/Ag_2O) and hence dissolution from iron rich $Nd_2Fe_{14}B$ phase is not feasible at applied potential of -3.3V. Hence, it is very likely that dissolution induced dealloying leads to leaching of residual iron from Ln-rich grains and grain boundary regimes. If the iron rich $Nd_2Fe_{14}B$ phase was not participating in the selective dissolution process under applied potential, it is expected to maintain its crystalline and morphological structure. Similarly, if the Ln-rich phase were selectively dissolving, it is expected to significantly alter the microstructural grain arrangements of Nd-Fe-B magnets. To evaluate the structural and chemical evolutions on Nd-Fe-B magnet upon selective oxidative dissolution, we performed Grazing Incidence X-ray diffraction (GIXRD) and SEM analysis. The GIXRD pattern (Figure S4) reveals no significant changes within the iron rich lattice of $Nd_2Fe_{14}B$ phase, indicating the dissolution is most likely from Ln-rich phases distributed across the Nd-Fe-B magnet. It is known that Ln-rich grain boundaries are likely to be enveloped with oxide layers, such as Nd_2O_3 and NdO_2 which could passivate against oxidative dissolution. Nevertheless, the major GIXRD peaks at 44° and 46° corresponding to Nd_2O_3 and at 43° corresponding to NdO_2 are disappearing when the applied potential becomes more negative (-3.3V), demonstrating that electrochemical stimuli can initiate and sustain selective Ln oxidation despite chemical heterogeneity of Nd-Fe-B magnets. Evidently, the SEM analysis reveals selective dissolution from Ln-rich phases with rate of dissolution depending on the applied potential and duration. For example, after 2hrs at -3.3V the preferential dissolution of Ln-rich grains resulting in voids and discontinuous distribution of $Nd_2Fe_{14}B$ phase. This implies that, after 2hrs of electrolytic dissolution the lack of continuous Ln-rich grains at the surface limits the Ln diffusion pathways and subsequently suppresses the dissolution rate which manifest as drop in current. Our results suggests that oxidative dissolution is solid-phase diffusion dependent and primarily involves the Ln-rich regions leaving the $Nd_2Fe_{14}B$ phase mostly intact, likely due to significantly shifted oxidation potentials of iron-rich grains. Nevertheless, considering the Ln-composition is primarily concentrated (~80% of total Ln composition in the magnet) in Ln-rich region (as shown in Figure 2) lack of iron-rich $Nd_2Fe_{14}B$ phase involvement in electrochemical dissolution doesn't impediment the overall extraction efficiency and could still render an efficient methodology provided concurrent electrodeposition of Ln elements can also be established. The dissolved Ln-elements under amperometric conditions are expected to undergo reduction reaction and establish electrodeposition as metallic alloy at Pt cathode. The Pt electrode was investigated by SEM and EDX as shown in Figure 5. A clearly distinguishable layers on both sides of Pt electrode confirms concurrent metal deposition process with amperometric dissolution conditions. Based on SEM-EDX data (Table S3), it is verified that the deposited layer predominantly contains Nd and Pr elements, with about 3:1 wt% Nd:Pr ratio.

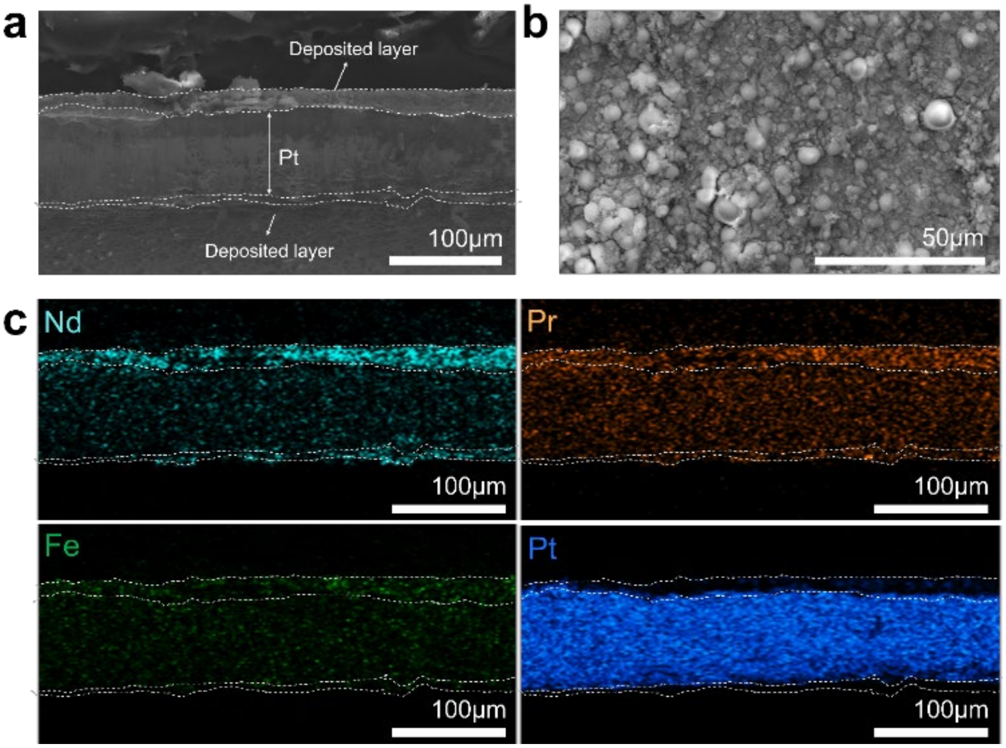

Figure 5. (a) Cross-sectional SEM images of the Pt electrode with two deposited layers on both sides by the amperometric dissolution and electrodeposition of Ln in 0.1M LiCl/DMF electrolyte at -3.3V, (b) SEM image of the Pt electrode showing surface morphology likely evolved from clustered nucleation of REEs during the deposition process, and (c) Cross- sectional chemical element maps from EDX analysis.

Interestingly, while the Fe is detected the Gd is not detected in the deposits. The absence of Gd agrees with ICP electrolyte analysis, whereas the Fe could be surface adsorption and/or metal deposition from co-leached Fe3+ species present in electrolyte. A closer look at the SEM images (Figure 5c and SI Figure 5) also reveals clustered particles ranging from submicron to few microns across the Pt surface. Both the nucleation kinetics and morphology of these clusters will depend on interfacial reactivity in addition to surface adsorption and diffusion of Ln elements.[23] In particular, parasitic reactivity between 9 depositing metallic lanthanides and electrolyte molecules can create passivating layers (such as oxide layer) which can limit further metal deposition process. Any such parasitic reactivity would primarily depend on electrochemical stability of solvent molecules. To study the chemical state of electrodeposited alloy and any possible parasitic reaction products, we performed XPS analysis.

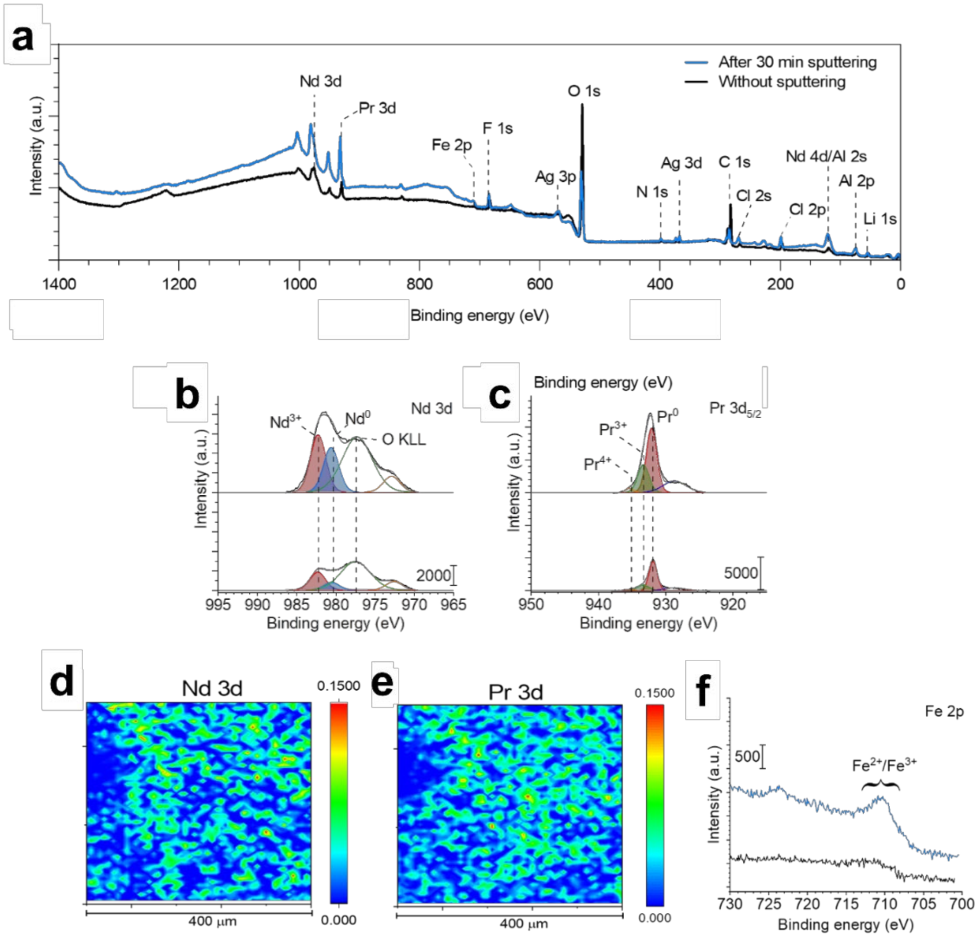

Figure 6. (a) XPS survey spectra collected on the Pt surface after the amperometric dissolution of Ln from the Nd-Fe-B magnet electrode and concurrent reduction at -3.3V for 24hr. The core-level spectra of (b) Nd *3d*, (c) Pr $3d_{5/2}$ before and after Ar sputtering revealing chemical state distribution across plating depth. The XPS images sputtered surface showing metallic (d) Nd *3d* and (e) Pr *3d* distribution on Pt electrode. (f) The iron co-deposition is very small (<1%) as confirmed by Fe *2p* core-level spectra before and after Ar sputtering.

The chemical compositional analysis derived from broad survey spectrum, shown in Figure 6a and 6f, reveals that Fe content on electrodeposited film is less than 1 at% along with Ag and Li representing the reference electrode and electrolyte components. Interestingly, small quantity of Fe is detected only after 30min of sputtering (Fig.6f), even then the Fe 2p core level signal suggests the presence of Fe^{2+}/Fe^{3+} ions rather than metallic iron. This suggests, the presence of iron is more likely to be surface chemisorption during the initial deposition process rather than continuous co-deposition with metallic lanthanides. It should be noted that, the Gd is also not observed in XPS spectrum (see SI Figure 6) and the 10 deposited layer is dominated by Nd and Pr element, which corroborates the EDS analysis (Fig.4 and Table S2). The high-resolution Nd $3d_{5/2}$ and Pr $3d_{5/2}$ shows both metallic and oxide forms, albeit with different compositional ratio of 72 wt.% and 28 wt.% for Nd and Pr respectively. The presence of oxide layer indicates two possible mechanisms, 1) electrolyte decomposition leading to interphase layer, and 2) surface oxidation during sample transfer to XPS measurements. It is expected that such procedural contamination during sample handling will be limited to oxidation of the surface layer and mostly unperturbed subsurface metallic layers. To test our hypothesis, we performed Ar sputtering to peel off the surface layer and probe the subsurface layers. After 5min of sputtering, the metal component of both Nd and Pr significantly increased (about 500 %) relative to the top surface layer. The significant drop in oxide components along the film depth suggests that at least most of the oxidation is part of procedural contamination and electrolyte is reasonably stable enough to support continuous metal deposition process. This result also corroborates the electrolyte stability evaluated by NMR analysis (Figure S3). The presence of both Nd and Pr in metallic phase across surface and subsurface suggests the possibility of didymium alloy formation during electrodeposition process. However, considering the clustered nucleation observed in SEM images (Fig.4c), it is possible to have single phase Nd and Pr metal particles forming separately but closely distributed across the Pt electrode. To test the chemical distribution of nucleated clusters, we performed imaging XPS on Nd $3d_{5/2}$ and Pr $3d_{5/2}$ peak positions as shown in Figure 6d & e. The clustering in metal deposition is clear in XPS imaging, with the Nd and Pr distribution regimes mostly matching, albeit with different intensity, suggesting likely didymium alloy formation. However, considering the spectral resolution limits of both EDS and imaging XPS, it is possible to have individual metallic phase nucleation due to local chemical potential variations during plating process. Overall, gaining control over charge transfer and transport processes would maximize the leaching and deposition efficiency of chemically and morphologically complex real-world magnets. Currently, we are planning further studies focusing on electrolyte development and electrochemical parameter controls to enhance the rate and selectivity of dissolution and deposition process.

4.0 References

(1) Julia W. Darcy, H. M. D. B., B. Mishra, B. Blanplain,; D. Apelian, a. M. H. E. "Challenges in Recycling End-of-Life Rare Earth Magnets". *The Journal of the Minerals, Metals & Materials Society* **2013**, *65* (11), 1381-1382. DOI: https://doi.org/10.1007/s11837-013-0783-0.

(2) Venkatesan, P.; Vander Hoogerstraete, T.; Binnemans, K.; Sun, Z.; Sietsma, J.; Yang, Y. "Selective Extraction of Rare-Earth Elements from NdFeB Magnets by a Room-Temperature Electrolysis Pretreatment Step". *ACS Sustainable Chemistry & Engineering* **2018**, *6* (7), 9375-9382. DOI: https://doi.org/10.1021/acssuschemeng.8b01707.

(3) Venkatesan, P.; Sun, Z. H. I.; Sietsma, J.; Yang, Y. "An environmentally friendly electro-oxidative approach to recover valuable elements from NdFeB magnet waste". *Separation and Purification Technology* **2018**, *191*, 384-391. DOI: https://doi.org/10.1016/j.seppur.2017.09.053.

(4) Venkatesan, P.; Vander Hoogerstraete, T.; Hennebel, T.; Binnemans, K.; Sietsma, J.; Yang, Y. "Selective electrochemical extraction of REEs from NdFeB magnet waste at room temperature". *Green Chemistry* **2018**, *20* (5), 1065-1073, 10.1039/C7GC03296J. DOI: https://doi.org/10.1039/C7GC03296J.

(5) Kumari, A.; Dipali; Randhawa, N. S.; Sahu, S. K. "Electrochemical treatment of spent NdFeB magnet in organic acid for recovery of rare earths and other metal values". *Journal of Cleaner Production* **2021**, *309*, 127393. DOI: https://doi.org/10.1016/j.jclepro.2021.127393.

(6) Belfqueh, S.; Seron, A.; Chapron, S.; Arrachart, G.; Menad, N. "Evaluating organic acids as alternative leaching reagents for rare earth elements recovery from NdFeB magnets". *Journal of Rare Earths* **2023**, *41* (4), 621-631. DOI: https://doi.org/10.1016/j.jre.2022.04.027.

(7) Dewulf, B.; Batchu, N. K.; Binnemans, K. "Enhanced Separation of Neodymium and Dysprosium by Nonaqueous Solvent Extraction from a Polyethylene Glycol 200 Phase Using the Neutral Extractant Cyanex 923". *ACS Sustainable Chemistry & Engineering* **2020**, *8* (51), 19032-19039. DOI: https://doi.org/10.1021/acssuschemeng.0c07207.

(8) Sun, P.-P.; Kim, D.-H.; Cho, S.-Y. "Separation of neodymium and dysprosium from nitrate solutions by solvent extraction with Cyanex272". *Minerals Engineering* **2018**, *118*, 9-15. DOI: https://doi.org/10.1016/j.mineng.2017.12.018.

(9) Kim, D.; Powell, L. E.; Delmau, L. H.; Peterson, E. S.; Herchenroeder, J.; Bhave, R. R. "Selective Extraction of Rare Earth Elements from Permanent Magnet Scraps with Membrane Solvent Extraction". *Environmental Science & Technology* **2015**, *49* (16), 9452-9459. DOI: https://doi.org/10.1021/acs.est.5b01306.

(10) Makarova, I.; Soboleva, E.; Osipenko, M.; Kurilo, I.; Laatikainen, M.; Repo, E. "Electrochemical leaching of rare-earth elements from spent NdFeB magnets". *Hydrometallurgy* **2020**, *192*, 105264. DOI: https://doi.org/10.1016/j.hydromet.2020.105264.

(11) Kamimoto, Y.; Itoh, T.; Kuroda, K.; Ichino, R. "Recovery of rare-earth elements from neodymium magnets using molten salt electrolysis". *Journal of Material Cycles and Waste Management* **2017**, *19* (3), 1017-1021. DOI: https://doi.org/10.1007/s10163-016-0563-3.

(12) Yang, Y.; Lan, C.; Wang, Y.; Zhao, Z.; Li, B. "Recycling of ultrafine NdFeB waste by the selective precipitation of rare earth and the electrodeposition of iron in hydrofluoric acid". *Separation and Purification Technology* **2020**, *230*, 115870. DOI: https://doi.org/10.1016/j.seppur.2019.115870.

(13) Geysens, P.; Lin, P.-C.; Fransaer, J.; Binnemans, K. "Electrodeposition of neodymium and dysprosium from organic electrolytes". *Physical Chemistry Chemical Physics* **2021**, *23* (15), 9070-9079, 10.1039/D0CP06606K. DOI: https://doi.org/10.1039/D0CP06606K.

(14) Burzo, E. "Permanent magnets based on R-Fe-B and R-Fe-C alloys". *Reports on Progress in Physics* **1998**, *61* (9), 1099. DOI: 10.1088/0034-4885/61/9/001.

(15) Sieradzki, K.; Dimitrov, N.; Movrin, D.; McCall, C.; Vasiljevic, N.; Erlebacher, J. "The Dealloying Critical Potential". *Journal of The Electrochemical Society* **2002**, *149* (8), B370. DOI: 10.1149/1.1492288.

(16) Tang, W.; Zhou, S.; Wang, R.; Graham, C. D., Jr. "An investigation of the Nd-rich phases in the Nd-Fe-B system". *Journal of Applied Physics* **1988**, *64* (10), 5516-5518. DOI: https://doi.org/10.1063/1.342321 (acccessed 7/18/2023).

(17) Wang, S. C.; Li, Y. "In situ TEM study of Nd-rich phase in NdFeB magnet". *Journal of Magnetism and Magnetic Materials* **2005**, *285* (1), 177-182. DOI: https://doi.org/10.1016/j.jmmm.2004.07.035.

(18) Mo, W.; Zhang, L.; Liu, Q.; Shan, A.; Wu, J.; Komuro, M. "Dependence of the crystal structure of the Nd-rich phase on oxygen content in an Nd–Fe–B sintered magnet". *Scripta Materialia* **2008**, *59* (2), 179-182. DOI: https://doi.org/10.1016/j.scriptamat.2008.03.004.

(19) Lu, Y.; Zhong, S.; Yang, M.; Wang, C.; Yang, L.; Li, L.; Yang, B. "Nd-Fe-B Magnets: The Gradient Change of Microstructures and the Diffusion Principle after Grain Boundary Diffusion Process". In *Materials*, 2019; Vol. 12. DOI: 10.3390/ma12233881.

(20) Liu, Z.; He, J.; Ramanujan, R. "Significant progress of grain boundary diffusion process for cost-effective rare earth permanent magnets: A review". *Materials & Design* **2021**, *209*, 110004. DOI: https://doi.org/10.1016/j.matdes.2021.110004.

(21) Kitagawa, J.; Uemura, R. "Rare Earth Extraction from NdFeB Magnet Using a Closed-Loop Acid Process". *Scientific Reports* **2017**, *7* (1), 8039. DOI: 10.1038/s41598-017-08629-z.

(22) Önal, M. A. R.; Borra, C. R.; Guo, M.; Blanpain, B.; Van Gerven, T. "Recycling of NdFeB Magnets Using Sulfation, Selective Roasting, and Water Leaching". *Journal of Sustainable Metallurgy* **2015**, *1* (3), 199-215. DOI: 10.1007/s40831-015-0021-9.

(23) Radisic, A.; Vereecken, P. M.; Hannon, J. B.; Searson, P. C.; Ross, F. M. "Quantifying Electrochemical Nucleation and Growth of Nanoscale Clusters Using Real-Time Kinetic Data". *Nano Letters* **2006**, *6* (2), 238-242. DOI: 10.1021/nl052175i.

Appendix A – Supplementary Information

Electrochemical measurements

To selectively electro-leach lanthanide (Ln) ions, cyclic voltammograms over a wide potential range (-3.25V – 1.0V) were performed for ten consecutive cycles at 20 mV/s scan rate within 0.1 M LiCl in DMF based electrolyte on a Pt electrode with NdFeB magnet as counter electrode (Fig S2a). The reduction reactions of Nd^{3+} and Nd^{2+} are observed in all ten cycles at -2.9 V and -2.58 V, respectively. Furthermore, the reduction reaction of borate is observed in the first cycle at -1.11 V and the reduction reaction of iron (II) ion is observed at -0.72 V. The reductions of aluminum and nickel are also observed at -1.66 V and -0.72 V, respectively. Despite purchasing a commercially produced uncoated magnet, the nickel and aluminum observed in the experiments suggest there may have been a protective coating on the magnet to avoid surface oxidization. The measured voltages and corresponding reduction reactions are listed in Table S1. The CVs confirm feasibility of electro-leaching Ln from NdFeB magnet and the LiCl/DMF electrolyte is sufficiently stable in with wide potential range used to reduce Ln ions on Pt electrode. The boundary between the nascent (upper shiny) and electrodeposited (mat) regions of the Pt electrode was clearly distinguishable visually as shown in Figs. S2b and S2d, respectively. SEM images of the two regions also showed rough surface with lots of deposits post-CV (Fig S2e) cycling compared to pristine Pt electrode pre-CV (Fig S2c).

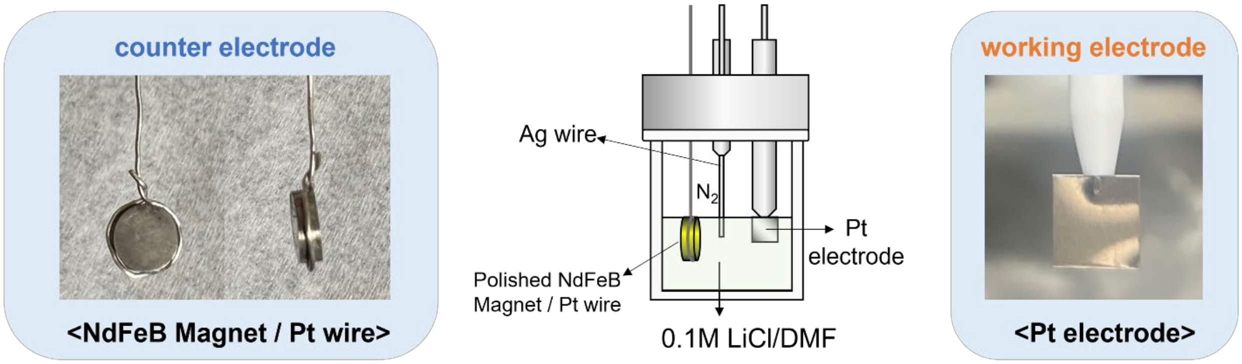

Figure 7. (a) Digital photograph of the polished Nd-Fe-B magnet tied with platinum wire as a counter electrode and the schematic illustration of the electrochemical cell equipped with a Pt plate as a working electrode, silver wire as a pseudo reference electrode in 0.1M LiCl/DMF electrolyte.

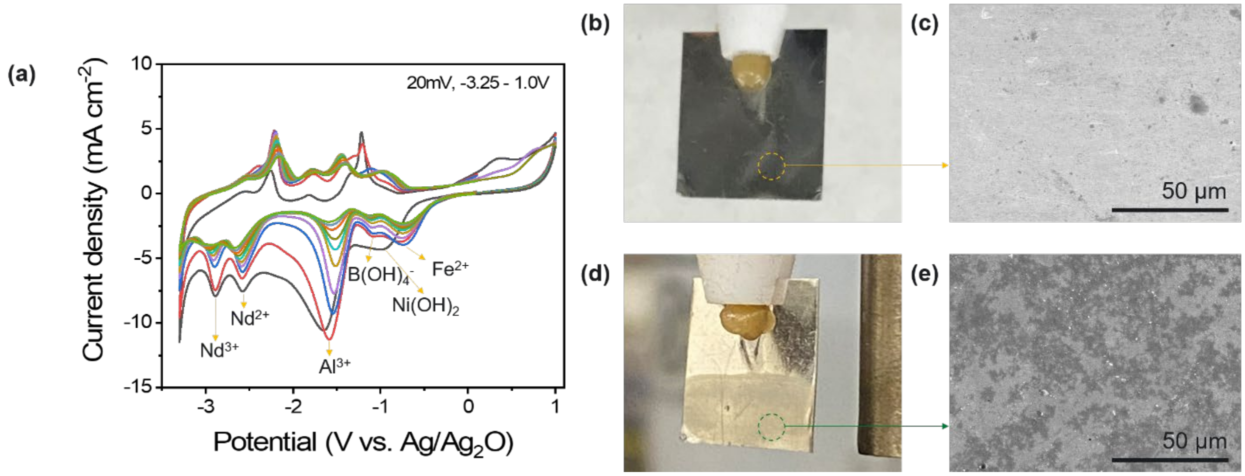

Figure 8. (a) Cyclic voltammograms of NdFeB magnet vs. Pt counter electrode performed at a scan rate of 20 mV s^{-1} for 10 cycles in the potential range -3.5V – 1.0V vs. Ag/Ag$_2$O with 0.1 M LiCl in DMF electrolyte. Digital photographs and SEM images of the Pt electrode before (b and c) and after (d and e) CV cycles. After CV images clearly show electrodeposited material on Pt surface.

E_{Ag/Ag_2O}	**E°$_{(calc)}$**	**E°**	**Reduction reaction**
-2.9 V	-2.56 V	-2.7 V	$Nd^{3+} + e^{-} \leftrightarrow Nd^{2+}$
-2.58 V	-2.24 V	-2.323 V	$Nd^{3+} + 3e^{-} \leftrightarrow Nd(s)$
		-2.1 V	$Nd^{2+} + 2e^{-} \leftrightarrow Nd(s)$
-1.61 V; -2.03 V to 1.3 V	-1.27 V; -1.68 V to -0.96 V	-1.66 V	$Al^{3+} + 3e^{-} \leftrightarrow Al(s)$
-1.11 V	-0.77 V	-0.89 V	$B(OH)_3 + 3H^{+} + 3e^{-} \leftrightarrow B(s) + 3H_2O(l)$
-0.95 V	-0.61 V	-0.72 V	$Ni(OH)_2(s) + 2e^{-} \leftrightarrow Ni\ (s) + 2OH^{-}$
-0.72 V	-0.38 V	-0.44 V	$Fe^{2+} + 2e^{-} \leftrightarrow Fe(s)$
0.74 V	1.08 V	1.19 V	$Pt^{2+} + 2e^{-} \leftrightarrow Pt(s)$

Table 1. Potential values and corresponding reduction reactions observed in cyclic voltammogram. Potential values of reduction peaks observed during first three CV cycles, reported along with calculated potential values using modified Nernst equation, and standard reduction potential values with corresponding reactions.

		Nd	Fe	Gd	Pr	O	Cu
a		19.1	67.1	7.4	4.5	0.9	0.8
b	1	52.8	9.6	6.9	15.9	0.7	14.2
	2	36.4	25.1	14.4	8.1	14.7	1.4

Table 2. SEM-EDX analysis of the polished Nd-Fe-B magnet.

NMR analysis

The ^{13}C and ^{1}H Nuclear magnetic resonance (NMR) spectra were recorded on a 500 MHz (^{1}H NMR resonance) spectrometer (Agilent, USA) at 25 °C with a 5-mm HX probe. The ^{13}C NMR spectra obtained at 125.715 MHz under broadband proton decoupling with a 90 degree pulse length of 9 µs and relaxation delay of 3 s. For ^{1}H NMR at 499.909 MHz, the 45 degree pulse length and the repetition delay were 3.8 µs and 5 s, respectively. 7Li NMR spectra were obtained at 194.298 MHz with the 90 degree pulse with 12 µs and repetition delay of 2 s. Both ^{1}H and ^{13}C chemical shifts were calibrated with tetramethylsilane (TMS) of 0 ppm as external standard.

Absence of new peaks, after 24hr constant potential amperometry condition, suggests that the LiCl/DMF solution is relatively stable to be used for recovery of REEs (Figure S3(a) and (b)). In addition, all NMR spectra (^{1}H, ^{13}C and ^{7}Li) showed that the gradual shift to higher frequency (larger chemical shift) due to the increase of the concentration of dissolving paramagnetic Ln ions during the constant potential amperometry. For example, the chemical shift differences of ^{1}H and ^{7}Li resonances between the samples before taking the amperometry (0.1 M LiCl) and after 24 h of amperometry (-3.3V, 24 h) were 22.35 and 8.86 Hz, respectively, suggesting most dissolved Nd ions solvated by DMF solvent molecules and minimally affect the existing lithium solvation structure and subsequently its diffusion process, which dictates overall ionic conductivity of the electrolyte. This can also be confirmed from the inset of Figure S3(c), which showed a minimal change in the line width (FWHH) while the chemical shifts of the ^{7}Li NMR spectra shifted to the higher frequency (more paramagnetic) as the increase of the time for the constant potential amperometry.

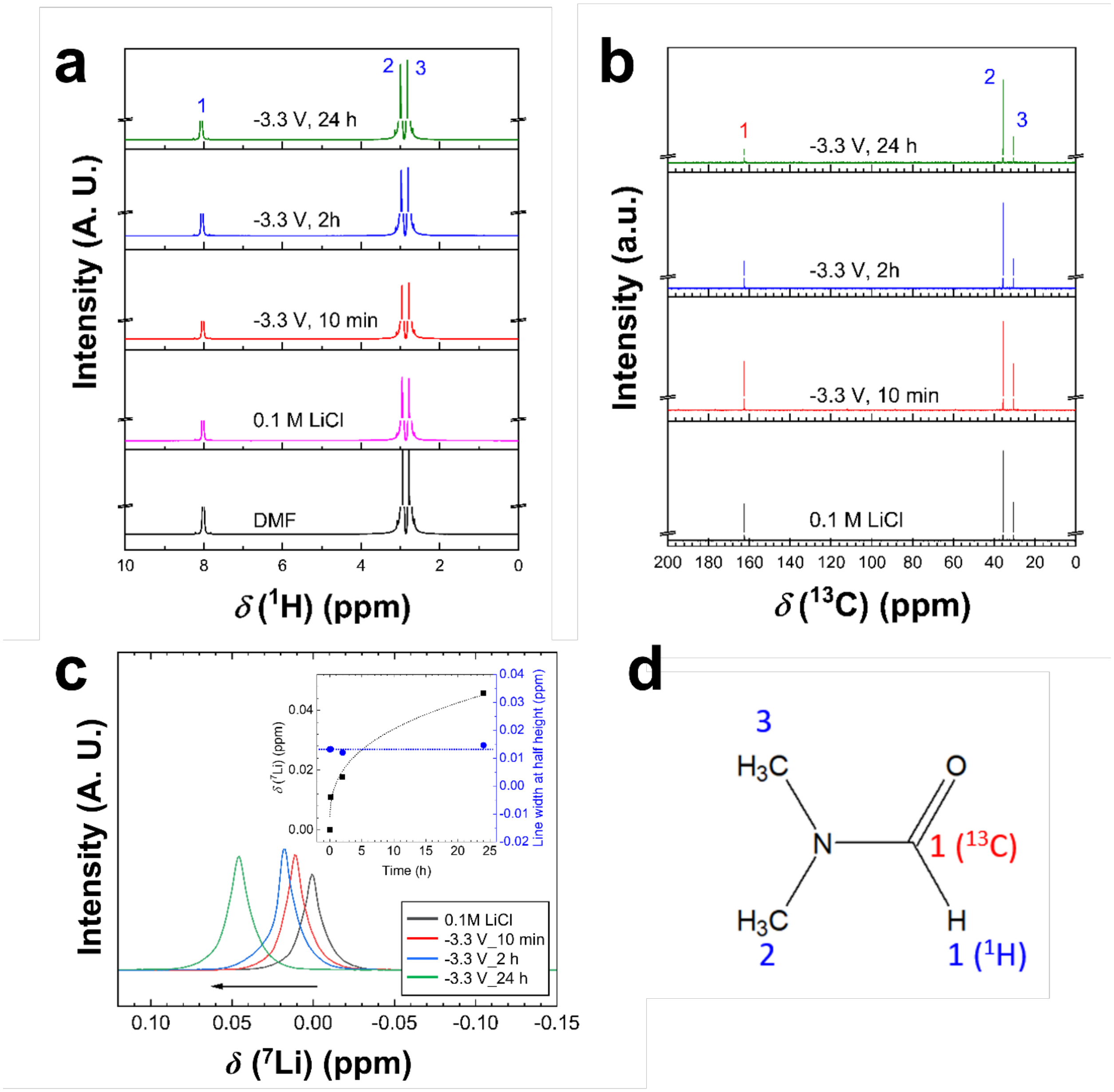

Figure 9. Time-dependent (10 min to 24 hours) nuclear magnetic resonance (NMR) spectra (a) 1H, (b) 13C, and (c) 7Li of the 0.1 M LiCl/DMF electrolyte after the constant potential amperometry at -3.3 V. In the inset of (c), the paramagnetic induced chemical shift and FWHM of 7Li NMR spectra as function of the time for the constant potential amperometery shows the increase in the concentration of the dissolved Nd ions in electrolyte. The dotted-lines are the guide to the eye. (d) The structure of dimethylformamide, and the numerals label the ^{1}H and ^{13}C resonances.

GIXRD analysis

To investigate the electrochemical selective leaching of Ln from the magnet electrodes employed for the potentiaostat measurements at different potentials for 2h, Grazing Incidence X-ray diffraction (GIXRD) was carried out. A fixed 5° incident angle was used to enable the penetration of 500 nm on the NdFeB magnet surface with 50-µm-diameter collimator. The GIXRD enabled the detection of smaller structural changes in surface layer compared to conventional XRD. Phase matching was carried out using JADE v.9.5.1 (Materials Data, Inc.) equipped with the 2019 PDF4+ database from ICDD (International Centre for Diffraction Data, Newtown Square, PA).

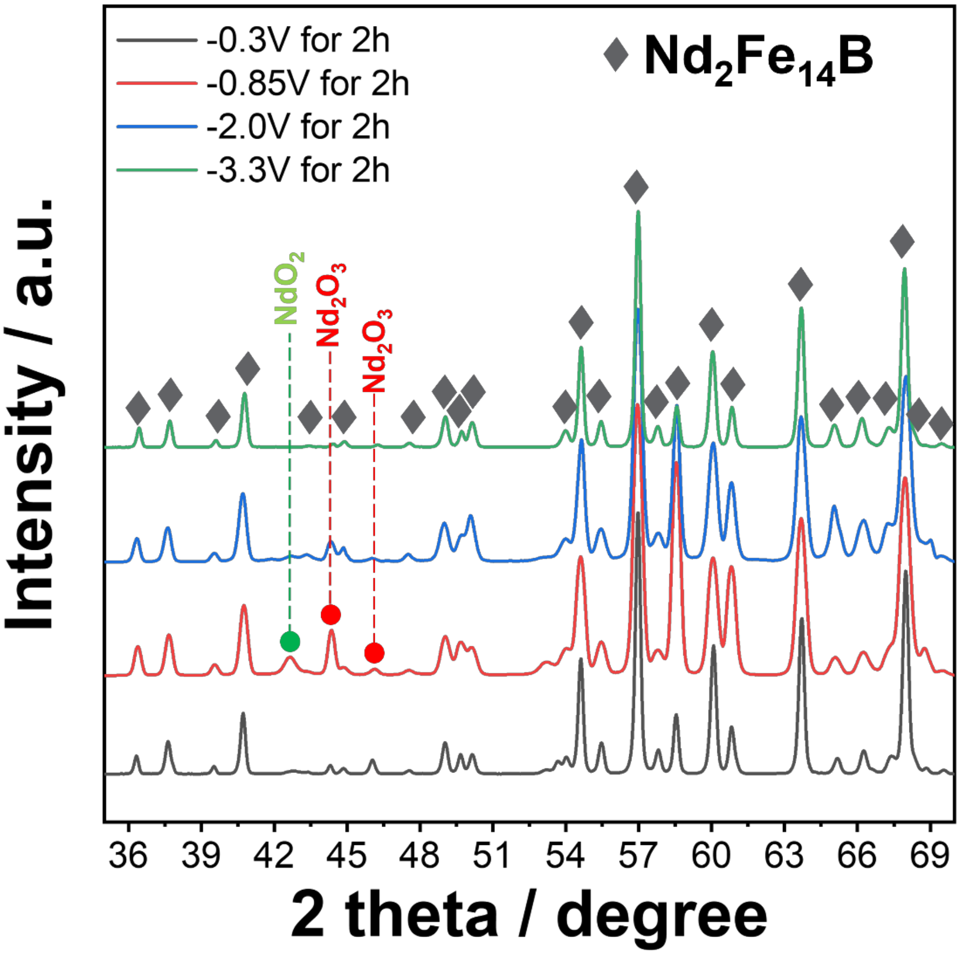

Figure 10. GIXRD patterns of the polished magnet electrodes after the amperometric dissolution of Ln in 0.1M LiCl/DMF electrolyte measured with Pt counter electrode and Ag pseudo reference electrodes at different potentials for 2 hours.

Morphological evolutions of metal deposition by SEM

To investigate the Ln metal alloy electrodeposition mechanisms and morphology on Pt electrodes from the dissolved Ln ions in the electrolytes we employed Scanning Electron Microscope (SEM). During the initial 10min deposition (Fig. S6b), the surface roughness of Pt electrode increases (Fig. S6a) suggesting distributed nucleation of Ln. After 2hr, the deposited Ln layer evolves to be a thicker discontinuous film consisting of the packed small particles grown across the surface. These observations are well matched with the increasing amperometric current (Fig. 3a) of the Pt electrode at -3.3V from the beginning of the measurement until 2 hours likely representing the nucleation and continuous growth of discontinuous Ln layer. Fig. S6d reveals that after 24 hours, with increased concentration of Ln ions (Fig. 3b in main text) in the electrolyte, the clustered particles of Ln metal alloys ranging from submicron to few microns develops across the Pt surface.

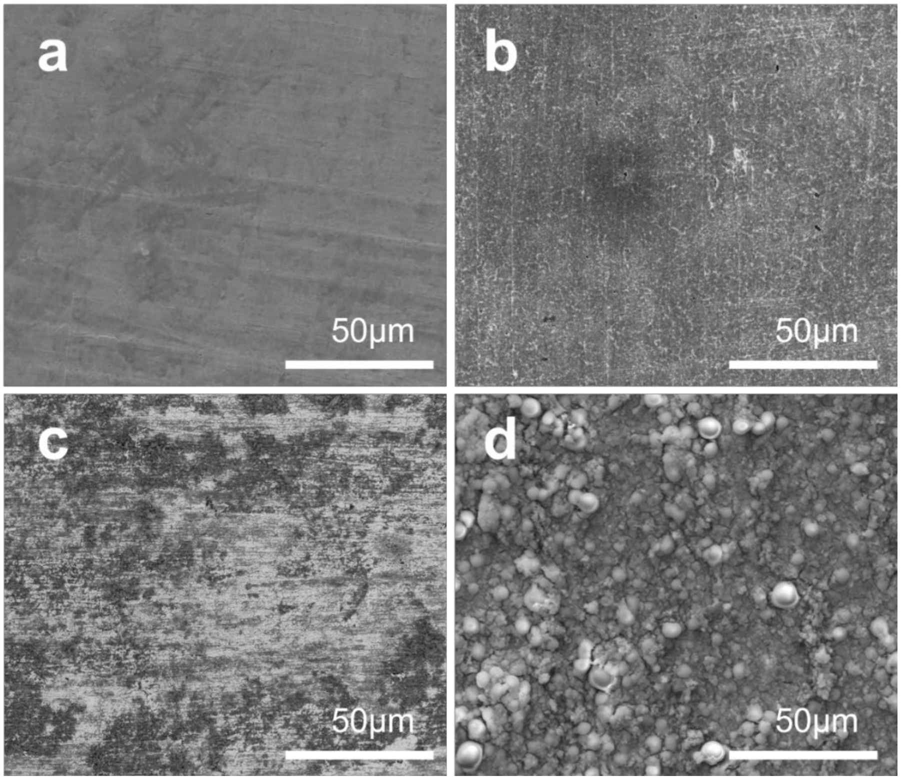

Figure 11. SEM images of the Pt electrode surfaces after the electrodeposition in 0.1M LiCl/DMF electrolytes by potentialstatic measurement at -3.3V for (a) 0, (b) 10min, (c) 2 h, and (d) 24 h, respectively.

	Pt electrode at -3.3V for 2h								
	Pt	C	O	Nd	Al	Pr	Cl	Fe	Ag
Wt.%	44.7	32.0	16.9	1.8	1.2	0.7	0.5	0.5	0.3

Table 3. SEM-EDX analysis of the elements detected on the cross-section of Pt electrode measured with the magnet working electrode in 0.1M LiCl/DMF electrolyte at -3.3V for 2h.

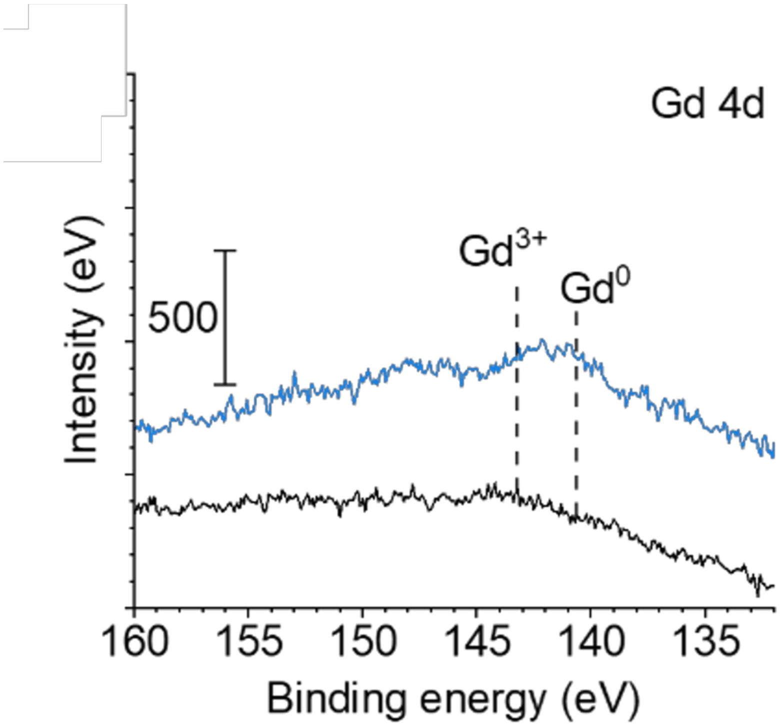

Figure S6. (a) XPS core-level spectra of Gd 4d before and after Ar sputtering revealing chemical state distribution across plating depth collected on the Pt surface after the amperometric dissolution of Ln from the Nd-Fe-B magnet electrode and concurrent reduction at -3.3V for 24hr.

Pacific Northwest
National Laboratory

902 Battelle Boulevard
P.O. Box 999
Richland, WA 99354

1-888-375-PNNL (7665)

www.pnnl.gov